Electrochemical detection of ultra-trace (pico-molar) levels of Hg^{2+} using a silver nanoparticle-modified glassy carbon electrode

Alex L. Suherman[1], Kamonwad Ngamchuea[1], Eden E. L. Tanner[1], Stanislav V. Sokolov[1], Jennifer Holter[2], Neil P. Young[2], Richard G. Compton[1,*]

[1] Department of Chemistry, Physical and Theoretical Chemistry Laboratory, University of Oxford, South Parks Road, Oxford OX1 3QZ, United Kingdom

[2] Department of Materials, University of Oxford, Parks Road, OX1 3PH, UK

*Corresponding Author:
Emails: richard.compton@chem.ox.ac.uk
Phone: +44(0) 1865 275957
Fax: +44 (0) 1865 275410

Abstract

Ultra-trace levels of Hg^{2+} have been quantified by undertaking linear sweep voltammetry with silver nanoparticle-modified glassy carbon electrode (AgNP-GCE) in aqueous solutions containing Hg^{2+}. This is achieved by monitoring the change in the silver stripping peak with Hg^{2+} concentration resulting from the galvanic displacement of silver by mercury: $Ag(np) + ½\ Hg^{2+}(aq) \rightarrow Ag^{+}(aq) + ½\ Hg(l)$. This facile and reproducible detection method exhibits an excellent linear dynamic range of 100.0 pM-10.0 nM Hg^{2+} concentration with $R^2 = 0.982$. The limit of detection (LoD) based on 3σ is 28 pM Hg^{2+}, whilst the lowest detectable level for quantification purposes is 100.0 pM. This method is appropriate for routine environmental monitoring and drinking water quality assessment since the guideline value set by the US Environmental Protection Agency (EPA) for inorganic mercury in drinking water is 0.002 mg L^{-1} (10 nM).

Keywords: ultra-trace level, Hg^{2+}, silver nanoparticle, glassy carbon, linear sweep voltammetry

1. Introduction

Exposure to mercury by the consumption of contaminated drinking water and food products may result in mortality, reproductive failure and other health effects in humans[1-4]. There is an increasing awareness and necessity for detection of mercury and is considered by the World Health Organization (WHO) as one of the top ten chemicals or groups of chemicals of major public health concern[1].

The WHO and the US Environmental Protection Agency (EPA) have issued guideline values for drinking water quality of 30 nM[5] and 10 nM[6] for inorganic mercury respectively. The development of a highly sensitive detection method that is reliable and simple for the routine detection of mercury in drinking water and the oil-and-gas industry is urgently needed. Currently, common detection methods for mercury include UV-Vis spectrophotometry[7], atomic absorption spectrometry (AAS)[8], cold vapour atomic absorption spectrometry (CVAAS)[9], atomic emission spectrometry (AES)[10], atomic fluorescence spectrometry (AFS)[11], X-ray fluorescence spectrometry (XFS)[12], inductive coupled plasma mass spectrometry (ICP-MS)[13], colorimetric assay[14] and gas chromatography (GC)[15]. These generally have high sensitivity and selectivity. However, they require large sample volumes, bulky instrumentation and extensive sample pre-treatment processes that limit their application to *in situ* analysis[16,17].

Voltammetric techniques are a promising alternative for the determination of inorganic Hg^{2+} in aqueous samples due to their excellent sensitivity, relatively low cost and short analysis time. Voltammetric techniques have been performed using different electrodes, including graphite[17,18], carbon paste[19,20], glassy carbon[21,22], screen-printed carbon[23,24], gold[25-27], platinum[28], titanium dioxide[29] and silver[30]. Anodic stripping voltammetry (ASV) has been used to detect micromolar levels of Hg^{2+} deposited on titanium dioxide electrodes by photochemical reduction, but required significant preconcentration times to achieve reasonable sensitivity[29], whilst linear sweep voltammetry (LSV) has also been employed to detect trace (10^{-8}-10^{-6} M) level of Hg^{2+} on gold ultra-microelectrode arrays[27]. However, bulk gold, platinum and silver electrodes are not suitable for Hg^{2+} detection since they suffer from structural changes of their surface caused by amalgam formation. This phenomenon can lead to decreasing sensor performance and loss of reproducibility[31], whilst the sensitivity of unmodified carbon electrodes is generally low, and the detection limit and preconcentration times are not acceptable for routine analyses[16,17].

In this paper we use a glassy carbon electrode (GCE) modified by drop-casting silver nanoparticles (AgNPs) without further surface modification. The AgNPs interact with Hg^{2+} in the solution so as to galvanically dissolve Ag via the reaction Ag (np) + ½ Hg^{2+} (aq) → Ag^{+} (aq) + ½ Hg (l). This leads to the loss of the stripping signal associated with the AgNPs. The large surface area of the drop-casted AgNPs permits a high sensitivity analytical performance since only tiny amounts of Hg^{2+} are required to displace measurable amounts of silver. The use of nanoparticles thus permits the measurement of the loss of silver, which would not be possible with a bulk silver electrode. Our proposed protocol has potential to be applied to routine detection and quantification of Hg^{2+} for environmental monitoring and drinking water quality purposes with limit of detection of 28 pM.

2. Experimental Section

2.1. Chemicals Reagents

Mercury solutions were prepared from 0.050 M mercury(II) nitrate ($Hg(NO_3)_2$, Fluka-Sigma Aldrich) and were diluted in 0.1 M potassium nitrate (KNO_3, Sigma Aldrich, >99.5%). Different suspensions of AgNPs (5.0 x 10^{15} NP dm^{-3}) of two different sizes, batch "A" and batch "B" (see below), were synthesized using trisodium citrate as a capping agent[32], whilst a nominally "50 nm diameter" AgNPs suspension (Ag content of 0.02 mg mL^{-1}) was sourced commercially (nanoComposiX, San Diego, US). Where water is referred to, ultrapure water with resistivity not less than 18.2 M Ωcm at 298 K (Millipore, US) was used. 0.1 M KNO_3 was used as supporting electrolyte throughout.

2.2. Electrochemical Apparatus

A three-electrode system was used for all electrochemical measurements. The system consisted of a 1.49 ± 0.01 mm in radius glassy carbon working electrode (CH Instruments, Inc., USA), a 0.5 mm diameter platinum wire counter electrode (Goodfellow Cambridge Ltd., UK) and a standard MSE (Hg/Hg_2SO_4, K_2SO_4 (saturated), +0.62 V *vs* SHE) reference electrode (BAS Inc., Japan). Experiments were carried out within a Faraday cage at 25 ± 1 ◦C using a μ-Autolab III potentiostat (Eco-Chemie, Netherlands) interfaced to a PC using GPES (version 4.9) software for Windows. All analyte solutions were degassed with high purity N_2 stream (oxygen free, BOC Gases plc) for 5 min before measurement. The GCE was cleaned by mechanical polishing on soft lapping pads using diamond spray (Kemet, UK) of sizes 3, 1 and 0.1 micron, then rinsed with ultrapure water. In order to maintain reproducibility, after each measurement the GCE was rinsed thoroughly by ultrapure water and soaked in 1.0 M HCl for 1 hour followed by mechanical polishing as mentioned previously. The GCE was then sonicated in acetone and ultrapure water for 1 minute each to remove any adsorbed material.

2.3. Drop-Casting Method

The freshly polished GCE was modified by placing a known volume of the 5.0 x 10^{15} NP dm^{-3} citrate-capped AgNPs suspension onto the electrode surface and allowing the drop to dry under nitrogen gas flow. After drying, the AgNPs-modified electrode (AgNPs-GCE) was immediately used for electrochemical experiments.

2.4. Silver Nanoparticle Characterization

Size characterization of the AgNPs was carried out using a Transmission Electron Microscope (TEM), a JEOL 3000F instrument, which has a field-emission gun and is operated at 300 kV. Sample preparation consisted of modifying carbon grids by drop-casting suspensions of the nanoparticles and allowing them to dry. Different areas of the grid were imaged to ensure a representative view of the sample. ImageJ software developed at the National Institute of Health, USA was used to size the nanoparticles recorded on the TEM images.

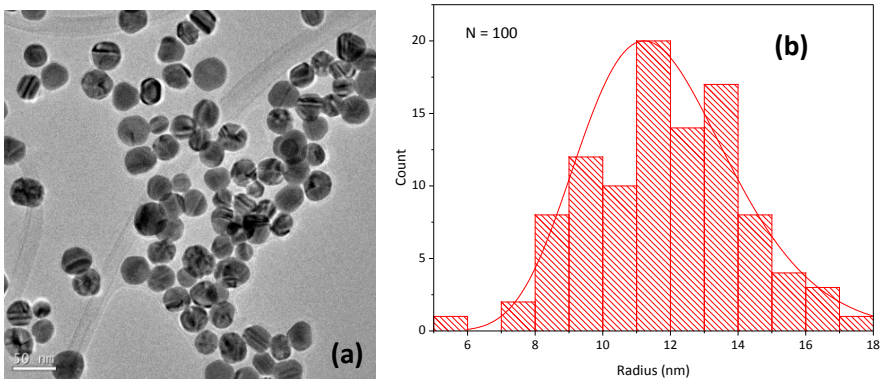

Figure 1. (a) TEM image of Batch "A" silver nanoparticles, (b) sizing histogram displaying the statistical distribution of the AgNPs radius size as extracted from TEM images of 100 NPs

Figure 1(a) shows a TEM image of batch "A" silver nanoparticles capped with trisodium citrate[32]. The data were processed to give a size distribution of the nanoparticle radii depicted in Figure 1(b) using OriginPro 2017 software for Windows. A lognormal curve is used to fit the data. The lognormal distribution of the particle size gave a mean radius of 11.9 (*/2.2) nm. For a lognormal distribution, the confidence interval is reported with a sign ''*/'' to indicate that it is obtained by multiplying or dividing the lognormal mean by the standard deviation, as compared to ''±'' for a normal distribution[33]. To assess the effect of size on Hg^{2+} detection, other sizes of AgNPs were used and sized to have a mean radius of 6.2 (*/1.5) nm and 22.5 (*/3.0) nm for batch "B" and nominally "50 nm diameter" respectively (see Supplementary Information, Figure S-1).

2.5. SEM Imaging of Dropcast Nanoparticles

The aggregation/agglomeration state of the particles was characterized using a JEOL JSM-6500F is a field-emission Scanning Electron Microscope (SEM) with an accelerating voltage of 5 kV using a secondary electron imaging mode. A glassy carbon (GC) plate was used as an electron imaging substrate. The preparation of the GC plate involved treatment with aqua-regia in order to provide a clean metal-free surface, rinsing with de-ionised water followed by the same polishing procedure used for electrode preparation as described above.

3. Results and Discussion

This section outlines the method for detection of ultra-trace levels of Hg^{2+} in aqueous solution by monitoring the reduction in size of the silver stripping peak from a Ag NP modified glassy carbon electrode with increasing Hg^{2+} concentration and exposure. First, optimisation of parameters that control the Ag stripping peak are discussed. Second, the addition and detection of ultra-trace levels of Hg^{2+} is undertaken by monitoring the magnitude of the silver stripping signal as a function of Hg^{2+} concentration. Third, the effect of the nanoparticle size towards the resulting signal or sensitivity is discussed.

3.1. Optimising the Silver Stripping Peak

First, the glassy carbon electrode (GCE) was modified with 11.9 (*/2.2) nm AgNPs. This size of NPs are used throughout except for a brief comparison with NPs of other sizes in Section 3.2 where they are shown to be optimal. After placing a droplet containing 2.5 x 10^{10} NPs leading to the formation of ca. 1.75 monolayer coverage (see below) onto the electrode, it was dried under nitrogen gas flow, resulting in a silver nanoparticle-modified glassy carbon electrode (AgNPs-GCE). The modified electrode was then immersed in 0.1 M KNO_3 and cyclic voltammetry (CV) was undertaken by sweeping the potential at a scan rate of 0.025 V s^{-1} from -0.50 V *vs* MSE to 0.40 V and back to -0.50 V (Figure 2).

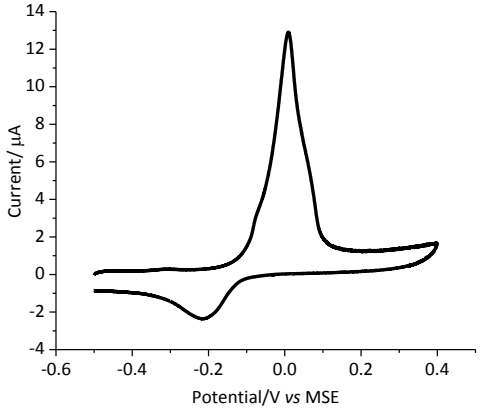

Figure 2. Cyclic voltammogram of GCE modified with 2.5 x 10^{10} Ag NPs (ca. 1.75 monolayer coverage, 11.9 (*/2.2) nm radius) in 0.10 M KNO_3 at a scan rate of 0.025 V s^{-1}.

On the first forward scan, a peak corresponding to Ag to Ag^+ oxidation was observed with a peak potential of 0.0095 V *vs* MSE with a peak height of 12.9 µA, whilst on the reverse scan a reductive peak appeared at -0.2 V *vs* MSE[34]. The latter is a result of the oxidised silver being re-reduced on the electrode. Integrating the forward peak results in a peak charge of 119 µC. The maximum charge (calculated from the number of nanoparticles dropcast and assuming that each atom transfers one electron) is *ca*. 1.8 mC, suggesting that *ca*. 7% was successfully stripped from the surface. This observation of partial stripping is consistent with previous literature reports documenting the oxidation of immobilised AgNPs on GCEs[35].

Next, a CV of thirty successive scans was undertaken on an electrode modified with 2.5 x 10^{10} NPs (Figure 3). Over thirty scans, the net oxidative peak charge was 340 µC, suggesting that *ca*. 19% of the silver had been stripped from the surface of the electrode. The cause of this incomplete stripping is discussed below.

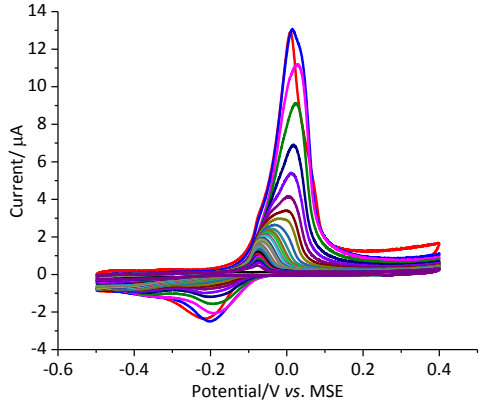

Figure 3. 30 successive voltammetric scans of a *ca*. 1.75 monolayer coverage of Ag NPs on a GCE in 0.1 M KNO_3 at a scan rate of 0.025 V s^{-1}.

The effect of surface coverage on the resultant silver stripping peak was then investigated by altering the number of nanoparticles used to modify the electrode. Five thicknesses of nanoparticles were examined – from approximately a monolayer to *ca*. 14 monolayers, crudely estimated assuming close packing of 91%[36]. As above, the various amounts of silver were each dropcast onto a clean GCE and the modified electrode was immersed in 0.1 M KNO_3. A linear sweep voltammetry (LSV) was then recorded at a scan rate of 0.1 V s^{-1} by sweeping the potential from -0.01 V to 0.5 V *vs* MSE and returning to -0.01 V (Figure 4).

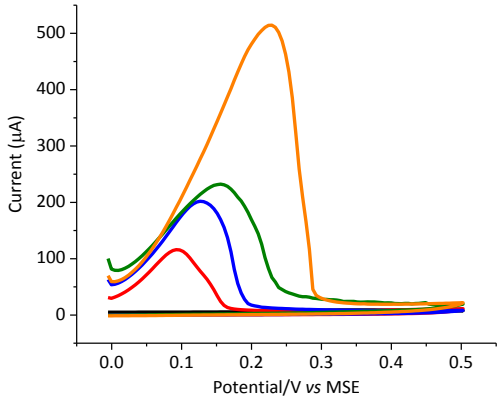

Figure 4. Linear sweep voltammograms of GCEs modified with 2.5 x 10^{10} Ag NPs (11.9 (*/2.2) nm radius) in 0.1 M KNO_3 with different drop cast masses: *ca*. monolayer (black), *ca*. 1.75 monolayers (red), *ca*. 3.5 monolayers (blue), *ca*. 7 monolayers (green), and *ca*. 14 monolayers (orange), at a scan rate of 0.1 V s^{-1}.

Table 1 reports the peak charge for each surface coverage, along with the theoretical maximum charge and the percentage of silver successfully stripped on the first scan. Compared with the maximum theoretical stripping, the *ca*. 1.75 monolayer coverage achieved a stripping efficiency of *ca*. 7% from the first scan. This was approximately constant for *ca*. 1.75 monolayer coverage and above suggesting either only partial contact of the film with the electrode or significant aggregation/agglomeration of the nanoparticles[37-40].

Table 1. Silver stripping peak charge at different drop cast masses

Surface Coverage Calculated from Dropcast (%)	**Silver Stripping Peak Charge (μC), *ca*.**	**Maximum Theoretical Peak Charge (mC), *ca*.**	**Efficiency of Stripping (%), *ca*.**
87 (*ca*. monolayer)	20.0	0.9	2
175 (*ca*. 1.75 monolayers)	119.0	1.8	7
350 (*ca*. 3.5 monolayers)	243.0	3.5	7
700 (*ca*. 7 monolayers)	384.3	6.9	5.5
1400 (*ca*. 14 monolayers)	811.6	13.8	6

To investigate the possible aggregation/agglomeration, a dropcasted layer on a GCE surface was studied using SEM. Figure 5 shows the SEM image from a single droplet containing 2.5 x 10^{10} Ag NPs, 11.9 (*/2.2) nm radius, which shows significant aggregation/agglomeration (see Supplementary Information Figure S-2). The aggregation/agglomeration of the particles drives the incomplete stripping of silver. Given the comparable efficiency of silver stripping peak and above drop casts, the *ca*. 1.75 monolayer drop cast mass was selected for all further experiments to minimize the amount of silver required.

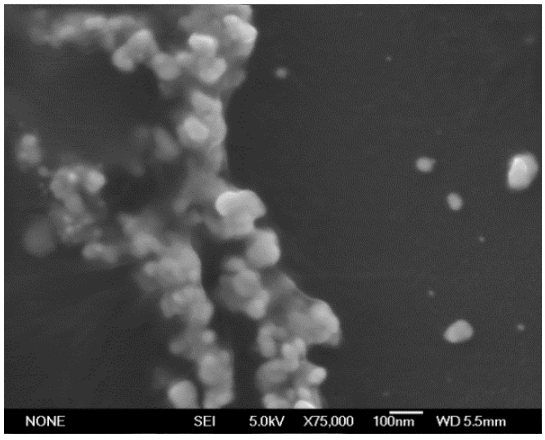

Figure 5. SEM image of 2.5 x 10^{10} Ag NPs with scanning magnification of 75,000x.

Next, the effect of scan rate was investigated. The AgNPs-GCE (2.5 x 10^{10} Ag NPs, 11.9 (*/2.2) nm radius) was immersed in 0.10 M KNO_3 and linear sweep voltammetry was undertaken by sweeping the potential at -0.01 V to 1.0 V *vs* MSE at a scan rate of 0.01, 0.02, 0.05 and 0.1 V s^{-1}. Figure 6 presents a plot of peak current *vs* scan rate with an R^2 = 0.98. The linear dependence of the peak current on the scan rate suggests that the species is surface bound (as expected from the dropcast method). For the analytical measurements reported below, a scan rate of 0.1 V s^{-1} was adopted for the reasons outlined in Section 3.2.

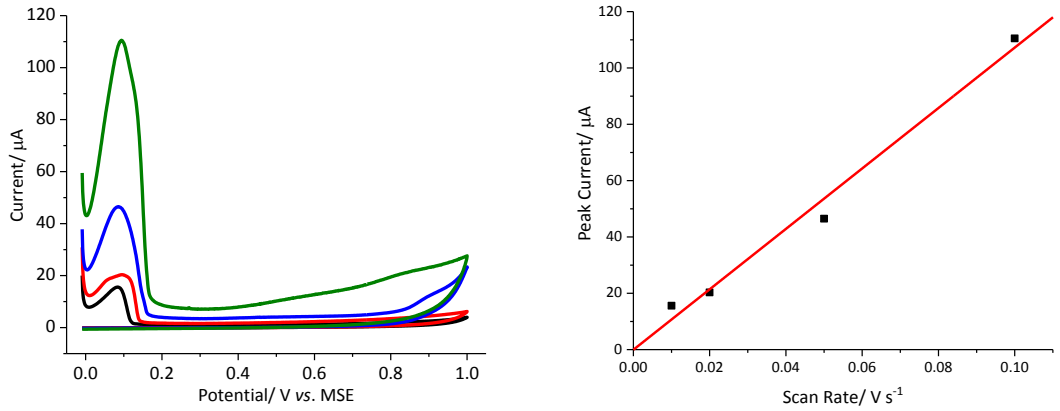

Figure 6. Linear sweep voltammograms of GCEs modified with 2.5 x 10^{10} Ag NPs (11.9 (*/2.2) nm radius) in 0.1 M KNO_3 with different scan rates: 0.01 V s^{-1} (black), 0.02 V s^{-1} (red), 0.05 V s^{-1} (blue), 0.1 V s^{-1} (green); and a plot of scan rate *vs* peak current.

To assess the reproducibility, a AgNPs-GCE (2.5 x 10^{10} Ag NPs, 11.9 (*/2.2) nm radius) was immersed in 0.1 M KNO_3 and held at a potential of -0.01 V *vs* MSE for 30 s. Following this, a linear sweep voltammetry was undertaken from -0.01 V to 1.0 V *vs* MSE at a scan rate of 0.1 V s^{-1} for three independent tests (Figure 7). The average peak current and peak charge are calculated to be 64.9 ± 0.3 μA and 59.6 ± 0.2 μC respectively. Figure 7 shows that a drop cast of 2.5 x 10^{10} Ag NPs, *ca*. 1.75 monolayer, shows excellent reproducibility of the silver stripping peak.

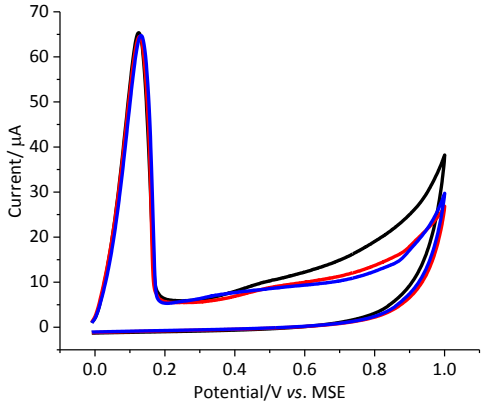

Figure 7. Reproducibility of three GCEs modified with 2.5 x 10^{10} Ag NPs (11.9 (*/2.2) nm radius) in 0.1 M KNO_3: 1st test (black), 2nd test (red), 3rd test (blue), at a scan rate of 0.1 V s^{-1}.

Finally, the length of time the electrode is immersed in the solution (hereafter referred to as the pre-stripping time) prior to the LSV being recorded plays a very important role to enable sensitivity of sensing performance (see below). To assess the effect of pre-stripping time on the silver stripping peak, the AgNPs-GCE was immersed in 0.1 M KNO_3 and a LSV was undertaken in three independent tests with accumulation times of 0, 30, 60, 100, 200, 300 and 500 seconds.

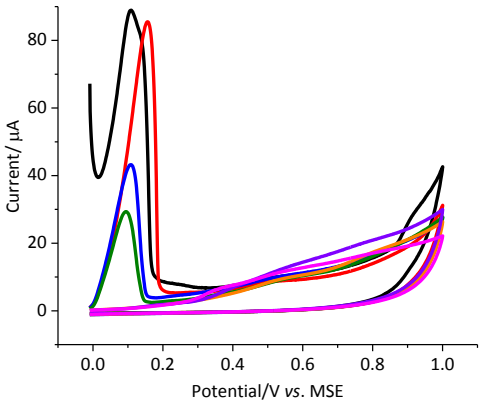

Figure 8. Linear sweep voltammograms of GCEs modified with 2.5 x 10^{10} Ag NPs (11.9 (*/2.2) nm radius) in 0.1 M KNO_3 with different accumulation times: 0 s (black), 30 s (red), 60 s (blue), 100 s (green), 200 s (orange), 300 s (purple), and 500 s (pink), at a scan rate of 0.1 V s^{-1}.

As shown in Figure 8, a well-defined Ag NPs stripping peak was found to decrease with time in solution. At an accumulation time of 0 s to 100 s, the peak is measurable, but at times of 200 s or above the peak is no longer discernible. This is as a result of the silver nanoparticles slowly dissolving from the electrode surface into the solution[41]. The dissolution is driven by the reduction of oxygen, which is even still present in micromolar concentrations after extensive bubbling with nitrogen[41]. Compared to other accumulation times, 30 s allows for time for the silver to react without compromising the sensitivity - thus 30 s was selected for further experiments.

3.2. Electrochemical Detection of Ultra-trace Level of Hg^{2+}

With the silver stripping signal optimised, the use of the Ag NP modified GC electrode to detect Hg^{2+} is next addressed. The stripping voltammetry detection approach has two steps; the first is a pre-stripping step, which involves holding the potential at a sufficiently negative value for a set length of time to allow the Hg^{2+} throughout the solution to react with the deposited silver without *electro*-deposition of mercury either in elemental form or as an amalgam. In this step, Hg^{2+} converts silver to Ag^{+} and so the amount of material available for stripping is diminished by an amount reflecting the concentration of Hg^{2+} in solution. The second step is the sweeping of the potential from -0.01 V to 1.0 V *vs* MSE which results in the electrochemical oxidation of Ag^{0} to Ag^{+} at the GCE surface, allowing the detection of the Ag left unreacted by Hg^{2+} and thus by comparison with the stripping signal in the absence of Hg^{2+}, the Hg^{2+} concentration in the solution.

First, the deposition and subsequent stripping of Hg^{2+} on a GCE in the absence of Ag NPs was investigated. A bare GCE was immersed in a solution containing 50.0 µM Hg^{2+} and held for 2 minutes at -0.5 V *vs* MSE such that Hg^{2+} deposition occurs[27]. Following this, a LSV was measured by sweeping the potential at a scan rate of 0.1 V s^{-1} from -0.50 V *vs* MSE to 1.0 V and back to -0.50 V (red line, Figure 9). Two oxidation peaks appear at peak potentials of 0.046 V and 0.222 V *vs* MSE, which correspond to mercury oxidation to Hg^{+} and from Hg^{+} to Hg^{2+} respectively[27,42]. The Hg(I) exists as Hg_2^{2+} (Hg-Hg). In the absence of Hg^{2+}, no features are present (blue line, Figure 9).

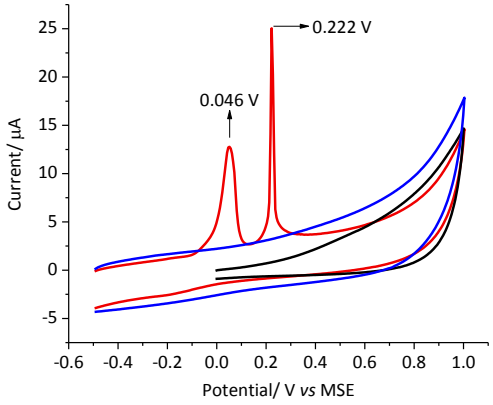

Figure 9. Linear sweep voltammograms of bare GCEs with starting potential of: -0.5 V in 0.1 M KNO_3 (blue), -0.5 V in 50.0 μM Hg^{2+} + 0.1 M KNO_3 (red), and -0.01 V in 50.0 μM Hg^{2+} + 0.1 M KNO_3 (black), at a scan rate of 0.1 V s^{-1}.

To assess the effect of starting potential, a bare GCE was immersed in a solution containing 50.0 μM Hg^{2+} and a LSV was recorded by sweeping the potential at a scan rate of 0.1 V s^{-1} from -0.01 V to 1.0 V *vs* MSE (black line, Figure 9). At these potentials, no mercury oxidation (Hg^{+} and Hg^{2+} stripping peaks) are observed. In the analytical determination of Hg^{2+} using Ag NPs, the starting potential must be positive enough to ensure that any oxidative features present are as a result of the interaction between silver and Hg^{2+}, and not from the oxidation of mercury, which was electrochemically deposited (as would occur if the electrode was held at sufficiently negative potentials), and negative enough such that measurement of the full silver stripping peak is visible. With these constraints in mind, a starting potential of -0.01 V was selected. At this potential Hg(l) is not deposited from Hg^{2+} nor are the Ag NPs stripped. Having optimised the starting potential, the analytical response of the modified electrode to different concentrations of Hg^{2+} was examined.

To assess the electroanalytical performance of AgNPs-GCE in the detection of ultra-trace levels of Hg^{2+}, a AgNPs-GCE was immersed in solutions of varying Hg^{2+} concentrations (100.0 pM to 10.0 nM) and after a wait period of 30 s (see above), a LSV was recorded at a scan rate of 0.1 V s^{-1} by sweeping the potential from -0.01 V *vs* MSE to 1.0 V and back to -0.01 V (Figure 10).

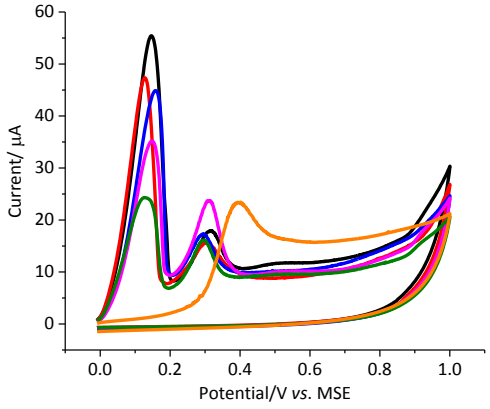

Figure 10. Representative voltammograms of AgNPs-GCEs (2.5 x 10^{10} Ag NPs (11.9 (*/2.2) nm radius) in 100.0 pM (black), 1.0 nM (red), 2.0 nM (blue), 4.0 nM (pink), 5.0 nM (green), 10.0 nM (orange) of Hg^{2+}, at scan rate of 0.1 V s^{-1}.

In each case, two peaks appear - the first at *ca.* 0.1 V vs MSE, and the second at *ca.* 0.3 V. The first peak corresponds to the silver stripping, as established in Section 3.1, whilst the second peak is related to mercury stripping, as investigated earlier in this Section. The decrease in the stripping peak as the Hg^{2+} concentration is increased, as explained above, is likely due to the reaction of Hg^{2+} with the silver nanoparticles, which at least until the Ag NPs are significantly oxidised, likely form an amalgam that is then oxidised at more positive potentials giving rise to the peak at 0.3 V *vs* MSE. Due to the fact that the mercury peak is heavily influenced by changes in kinetics and thermodynamics as the surface of the electrode changes with mercury deposition, the silver stripping peak was selected as the signal to be monitored, rather than the mercury oxidation peak.

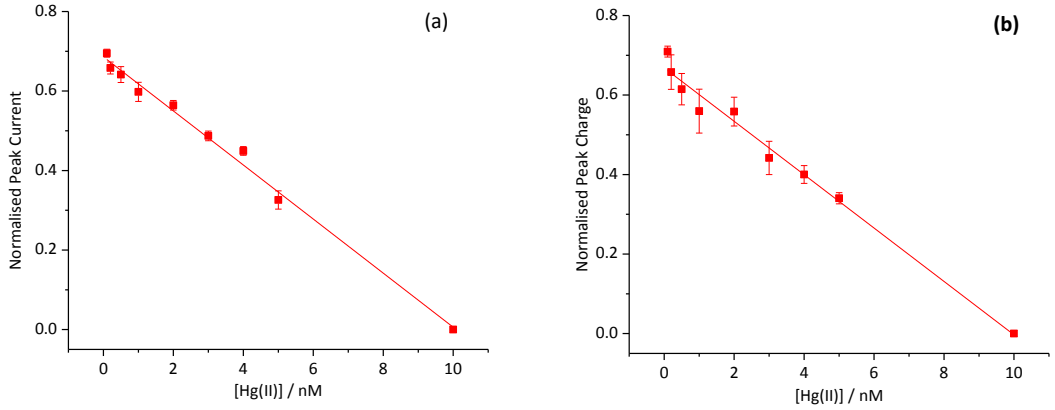

Figure 11. AgNPs-GCEs (2.5 x 10^{10} Ag NPs with 11.9 (*/2.2) nm radius) stripping peak in 100.0 pM-10.0 nM Hg^{2+} solutions in 0.1 M KNO_3: (a) normalised peak current, (b) normalised peak charge.

To assess the relationship between the silver stripping peak and Hg^{2+} concentration, a modified electrode (2.5 x 10^{10} Ag NPs, 11.9 (*/2.2) nm radius) was immersed in 0.1 M KNO_3 and different Hg^{2+} solutions. First, a AgNPs-GCE was immersed in a solution containing 100.0 pM Hg^{2+} and held at a potential of -0.01 V *vs* MSE for 30 s (see above). Following this, a LSV was recorded by sweeping the potential at a scan rate of 0.1 V s^{-1} from -0.01 V *vs* MSE to 1.0 V and back to -0.01 V. This procedure was repeated for 8 other different Hg^{2+} concentrations in the range of 200.0 pM to 10.0 nM. The resulting data are shown in Figure 11 with a "normalised stripping signal" plotted *vs* Hg^{2+} concentration. The reason for the normalisation is as follows. In the absence of Hg^{2+}, the silver stripping peak is affected by the accumulation time prior to the CV measurement, which allows sufficient time for the partial loss of silver through reduction of O_2. Note that micromolar concentrations of oxygen are present even after extensive bubbling with nitrogen[43]. The reduction of O_2 drives the oxidative dissolution of silver nanoparticles from the GCE surface, thus decreasing the silver stripping peak. In the presence of Hg^{2+}, the silver stripping peak is affected by *both* the loss during the accumulation time and the Hg^{2+} in the solution. In order to measure the silver stripping peak such that it only reflects the Hg^{2+} concentration, the signal was normalised by dividing the peak obtained in the presence of Hg^{2+} by the peak obtained in the absence of Hg^{2+} with no accumulation time. The ratio is the normalised peak current or peak charge. Figure 11 shows how the normalised stripping peak current and

the stripping charge on the first scan varies with the Hg^{2+} concentration. *Both* normalised peak current and peak charge ratios never reach a value of 1.0 because the accumulation time of 30 s enables the Ag NPs to react with Hg^{2+} in the solution and decreases the silver stripping peak. Both figures show linear trends of AgNPs-GCE in the range 100.0 pM to 10.0 nM Hg^{2+}. The linearity of measurement was found to be R^2 = 0.991 and R^2 = 0.982 for normalised peak current and normalised peak charge respectively.

Finally, the size of the nanoparticles used to modify the GC electrode were investigated in relation to the sensitivity of the measurement. To assess the effect of nanoparticle size on Hg^{2+} detection, suspensions of nanoparticles with a mean radius of 6.2 (*/1.50) nm (Batch "B") or 22.5 (*/3.05) nm (nominally "50 nm diameter", commercial product) were separately dropcast onto a GCE surface to give the same number of particles (2.5 x 10^{10} Ag NPs). All experiments were performed in 0.1 M KNO_3, 500.0 pM, 2.0 nM and 5.0 nM Hg^{2+} solutions. As shown in Supplementary Information Figure S-3 and Figure S-4, there is no significant effect of silver nanoparticle size on the resulting signal or sensitivity, suggesting that the process is controlled by diffusion of Hg^{2+} to the geometric area of the electrode rather than due to the surface area of silver available for oxidation. This is confirmed by analysis of variable surface coverages. A 2.5 x 10^{10} Ag NPs with radius of 11.9 (*/2.2) nm, 1.25 x 10^{10} Ag NPs with radius of 11.9 (*/2.2) nm and 2.5 x 10^{10} Ag NPs with radius of 6.2 (*/1.5) nm were dropcast to form a *ca*. 1.75 monolayer, *ca*. monolayer and *ca*. half monolayers at a GCE surface respectively. All experiments were performed both in 0.1 M KNO_3 and in 500.0 pM, 2.0 nM, 5.0 nM Hg^{2+} solutions and the surface coverage was not found to affect the slope of the detection curve (see Supplementary Information, Figure S-5 and Figure S-6).

In summary, our proposed method for detection of ultra-trace levels of Hg^{2+} in aqueous solution monitors the silver stripping peak from a dropcast *ca*. 1.75 monolayer of 11.9 (*/2.2) nm Ag NPs in response to the Hg^{2+} concentrations. The limit of detection (LoD) based on 3σ[44,45] was calculated to be 28 pM. The latter compares favourably with alternative methods[46-50], which also involve much lengthier pre-treatment processes.

4. Conclusions

We have developed a protocol for the detection of ultra-trace levels of Hg^{2+} in aqueous solutions undertaking linear sweep voltammetry using a AgNP-GCE. This protocol is appropriate for routine environmental monitoring and drinking water quality assessment with the use of a disposable screen-printed electrode. Our protocol is able to achieve a limit of detection of 28 pM and linear range of 100.0 pM to 10.0 nM meeting the 10 nM guidelines issued by EPA[6] for inorganic mercury in drinking water.

Acknowledgements

ALS thanks the Indonesia government through Indonesia Endowment Fund Scholarships for funding. We thank Ms Jessica Lees for the synthesis of the silver nanoparticles used in this study. The research leading to these results has received partial funding from the European Research Council under the European Union's Seventh Framework Programme (FP/2007-2013)/ERC Grant Agreement no. 320403).

Supporting Information

Detailed information on the TEM images and sizing histograms of silver nanoparticle at different sizes, SEM images of silver nanoparticle suspension (2.5 x 10^{10} Ag NPs), representative linear sweep voltammograms of AgNPs-GCEs at different nanoparticle sizes and surface coverages, and calculation of theoretical charge and surface coverage.

References

(1) WHO Fact Sheet **2017**. Accessed from http://www.who.int/mediacentre/factsheets/fs361/en/

(2) C. T. Driscoll, R. P. Mason, H. Chan, D. J. Jacob and N. Pirrone, *Environ. Sci. Technol.*, **2013**, 47, 4967-4983.

(3) S. M. Wilhelm and N. Bloom, *Fuel Process. Technol.*, **2000**, 63, 1-27.

(4) C. Gao and X. J. Huang, *TrAC, Trends Anal. Chem.*, **2013**, 51, 1-12.

(5) WHO Guidelines for Drinking-Water Quality, 4th Edition, **2011**. Accessed from http://www.who.int/water_sanitation_health/publications/2011/dwq_guidelines/en/

(6) EPA's Drinking Water Regulations for Mercury, EPA 816-F-09-004, **2009**. Accessed from https://safewater.zendesk.com/hc/en-us/articles/212076077-4-What-are-EPA-s-drinking-water-regulations-for-mercury-

(7) H. B. Ulusoy, R. Gürkan and S. Ulusoy, *Talanta*, **2012**, 88, 516-523.

(8) N. Rey-Raap and A. Gallardo, *Waste Manag.*, **2012**, 32, 944-948.

(9) E. Kopysc, K. Pyrzynska, S. Garbos and E. Bulska, *Anal. Sci.*, **2000**, 16, 1309-1312.

(10) M. D. Ioannidou, G. A. Zachariadis, A. N. Anthemidis and J. A. Stratis, *Talanta*, **2005**, 65, 92-97.

(11) L. Wu, Z. Long, L. Liu, Q. Zhou, Y. I. Lee and C. Zheng, *Talanta*, **2012**, 94, 146-151.

(12) P. R. Aranda, L. Colombo, E. Perino, I. E. De Vito and J. Raba, *X-Ray Spectrom.*, **2013**, 42.

(13) Y. Fang, Y. Pan, P. Li, M. Xue, F. Pei, W. Yang, N. Ma and Q. Hu, *Food Chem.*, **2016**, 213.

(14) P. Jarujamrus, M. Amatatongchai, A. Thima, T. Khongrangdee and C. Mongkontong, *Spectrochim. Acta - Part A Mol. Biomol. Spectrosc.*, **2015**, 142, 86-93.

(15) Y. Lin, Y. Yang, Y. Li, L. Yang, X. Hou, X. Feng and C. Zheng, *Environ. Sci. Technol.*, **2016**, 50, 2468-2476.

(16) M. Zaib, M. M. Athar, A. Saeed and U. Farooq, *Biosens. Bioelectron.*, **2015**, 74, 895-908.

(17) D. Martín-Yerga, M. B. González-García and A. Costa-García, *Talanta*, **2013**, 116, 1091-1104.

(18) F. El Aroui, S. Lahrich, A. Farahi, M. Achak, L. El Gaini, B. Manoun, M. Bakasse, A. Bouzidi and M. A. El Mhammedi, *J. Taiwan Inst. Chem. Eng.*, **2014**, 45, 2725-2732.

(19) J. Wang and M. Bonakdar, *Talanta*, **1988**, 35, 277-280.

(20) A. Afkhami, T. Madrakian, S. J. Sabounchei, M. Rezaei, S. Samiee and M. Pourshahbaz, *Sens. Actuators, B Chem.*, **2012**, 161, 542-548.

(21) J. Lu, X. He, X. Zeng, Q. Wan and Z. Zhang, *Talanta*, **2003**, 59, 553-560.

(22) M. Ghanei-Motlagh, R. Ghanei-Motlagh and V. K. Gupta, *Mater. Sci. Eng. C*, **2016**, 63, 367-375.

(23) S. Cinti, F. Santella, D. Moscone and F. Arduini, *Environ. Sci. Pollut. Res.*, **2016**, 23, 8192-8199.

(24) I. T. Somé, A. K. Sakira, D. Mertens, S. N. Ronkart and J. M. Kauffmann, *Talanta*, **2016**, 152, 335-340.

(25) Y. Bonfil, M. Brand and E. Kirowa-Eisner, *Anal. Chim. Acta*, **2000**, 424, 65-76.

(26) J. Wei, D. Yang, H. Chen, Y. Gao and H. Li, *Sens. Actuators, B Chem.*, **2014**, 190, 968-974.

(27) O. Ordeig, C. E. Banks, J. Del Campo, F. X. Muñoz and R. G. Compton, *Electroanalysis*, **2006**, 18, 573-578.

(28) J. M. Pinilla, L. Hernández and A. J. Conesa, *Anal. Chim. Acta*, **1996**, 319, 25-30.

(29) M. F. Suárez, A. Mills, R. G. Egdell and R. G. Compton, *Electroanalysis*, **2000**, 12, 413-419.A.

(30) Farahi, S. Lahrich, M. Achak, and M. A. El Mhammedi, *Sens. Bio-Sensing Res.*, **2015**, 4, 90-95.

(31) L. E. Barrosse-Antle, L. Xiao, G. G. Wildgoose, R. Baron, C. J. Salter, A. Crossley and R. G. Compton, *New J. Chem.*, **2007**, 31, 2071.

(32) J. C. Lees, J. Ellison, C. Batchelor-Mcauley, K. Tschulik, C. Damm, D. Omanovič and R. G. Compton, *ChemPhysChem*, **2013**, 14, 3895-3897.

(33) E. Limpert, W. a. Stahel and M. Abbt, *Bioscience*, **2001**, 51, 341.

(34) A. Zahid, A. Lashin, U. A. Rana, N. Al-Arifi, I. Ullah, D. D. Dionysiou, R. Qureshi, A. Waseem, H. B. Kraatz and A. Shah, *Electrochim. Acta*, **2016**, 190, 1007-1014.

(35) H. S. Toh, C. Batchelor-Mcauley, K. Tschulik, C. Damm and R. G. Compton, *Sens. Actuators, B Chem.*, **2014**, 193, 315-319.

(36) E. Kätelhön, W. Cheng, C. Batchelor-Mcauley, K. Tschulik and R. G. Compton, *ChemElectroChem*, **2014**, 1, 1057-1062.

(37) H. S. Toh, C. Batchelor-McAuley, K. Tschulik, M. Uhlemann, A. Crossley and R. G. Compton, *Nanoscale*, **2013**, 5, 4884-4893.

(38) S. J. Cloake, H. S. Toh, P. T. Lee, C. Salter, C. Johnston and R. G. Compton, *ChemistryOpen*, **2015**, 4, 22-26.

(39) H. S. Toh, K. Jurkschat and R. G. Compton, *Chem. - A Eur. J.*, **2015**, 21, 2998-3004.

(40) C. C. M. Neumann, E. Laborda, K. Tschulik, K. R. Ward and R. G. Compton, *Nano Res.*, **2013**, 6, 511-524.

(41) B. J. Plowman, K. Tschulik, E. Walport, N. P. Young and R. G. Compton, *Nanoscale*, **2015**, 7, 12361-12364.

(42) M. Korolczuk, Fresenius J. Anal. Chem. **1997**, 357, 389.

(43) R. O. D Clark, K. Ngamchuea, C. Batchelor-Mcauley, and R. G. Compton, *Electroanalysis*, **2017**, 29, 1-9.

(44) G. L. Long and J. D. Winefordner, *Anal. Chem.*, **1983**, 55, 712A.

(45) L. Laffont, T. Hezard, P. Gros, L. E. Heimberger, J. E. Sonke, P. Behra and D. Evrard, *Talanta*, **2015**, 141, 26-32.

(46) K. Tyszczuk-Rotko, I. Sadok and M. Barczak, *Microporous Mesoporous Mater.*, **2016**, 230, 109-117.

(47) S. Lahrich, B. Manoun and M. A. El Mhammedi, *Talanta*, **2016**, 149, 158-167.

(48) M. R. Mahmoudian, W. J. Basiruna and Y. Aliasac, *RSC Adv.*, **2016**, 6, 36459-36466.

(49) Y. Zhang, G. M. Zeng, L. Tang, J. Chen, Y. Zhu, X. X. He and Y. He, *Anal. Chem.*, **2015**, 87, 989-996.

(50) S. Amiri, A. Navaee, A. Salimi and R. Ahmadi, *Electrochem. commun.*, **2017**, 78, 21-25.

For TOC only

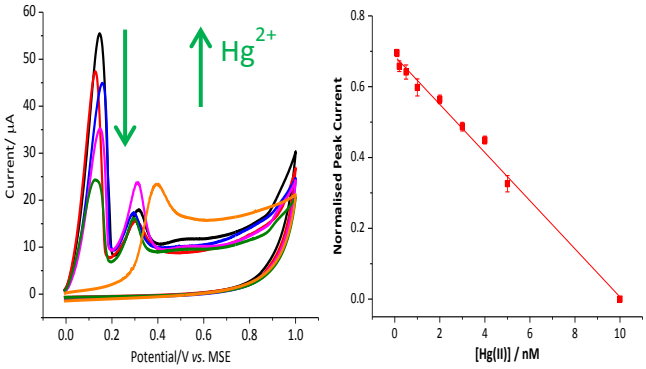
Hg2+
Current/ μA
Potential/V vs. MSE
Normalised Peak Current
[Hg(II)] / nM